HALO FROM COULOMB SCATTERING OF BEAM PARTICLES ON RESIDUAL GAS

NICOLAS PICHOFF [a,*], PIERRE-YVES BEAUVAIS [a]
and GÉRARD HAOUAT [b]

[a] *Commissariat á l'Energie Atomique – DSM/DAPNIA/SEA,
91191 Gif-sur-Yvette cedex, France;* [b] *Commissariat á l'Energie
Atomique – Direction des Applications Militaires,
BP12 91680 Bruyères-le-Châtel, France*

The contribution of Coulomb elastic scattering of beam particles on the residual gas to the beam halo development in a linear accelerator is studied. Starting from the basic differential cross section formula giving the probability of a particle to scatter at a given angle, we analyse the behaviour of those few particles which scatter at rather large angles and we estimate their proportion relative to the beam intensity. We present a transport code dedicated to the scattering of a beam on the residual gas, which we validate with an experiment in which the beam is transported through a drift space. We use then our code to simulate the transport of a beam matched to a uniform focusing channel and we show how the collisional halo develops. The code is finally used in order to establish the loss rate per meter in a high intensity linac. This loss rate is compared to the acceptable one.

Keywords: Halo; Scattering; Residual gas; High intensity linac; Experiment; Simulation

INTRODUCTION

The requirements of very high current linear electron and proton accelerators have increased considerably over the recent years. Beam losses are a main concern in the design of such machines. Experimental observations and theoretical predictions have shown the existence of a

---

* Corresponding author. E-mail: npichoff@cea.fr.

low-density halo surrounding the central core of a high-intensity beam. This halo not only leads to particle loss along the accelerator, but also can induce enough activity in the structures to complicate the maintenance of the machine. There are many contributions to the formation of the halo. Several theoretical studies have been undertaken to understand the formation of the halo through the dynamics of particle beam transport.[1,2] However, up to now, very few attempts have been made to study halo formation via interactions of beam particles with the residual gasses of the accelerator.

The scattering of particles in the residual gas of a circular accelerator is known to be crucial for the lifetime of the beam. It is essentially due to the billion kilometres covered by the beam before its extinction. However, in a linear accelerator, the distance is not so large, and it often seems reasonable to neglect the scattering effect on the residual gas. Moreover, in a linear accelerator, the vacuum quality is not as good as in a circular one, especially near the source where the beam energy is rather low, and the scattering effects can be important. This is why some physicists have studied the influence of scattering on the beam emittance growth, and have shown that its contribution is sometimes non-negligible.[3] They have used, in their studies, a statistical description of the scattering process (including multi-scattering), thereby neglecting the detailed effect of individual scattered particles on the beam profile.

We have undertaken an experimental study of halo formation and development around an intense (50 mA), low-energy (500 keV), low-emittance (0.6 $\pi \cdot$ mm $\cdot$ mrad, normalised) proton beam during its transport through a periodically focusing FODO channel.[4] The aim of this study is to understand the dynamics of an intense charged particle beam submitted to the interplay of internal, repulsive, space-charge forces and externally applied focusing forces.[5] In order to provide a coherent interpretation of this halo-producing process, it appears necessary to estimate the amount of halo produced by the scattering of beam particles on the residual gas, and to subtract it from the measured data.

Analysing the basic scattering process, we show that its effect is not negligible in the case of our experiment. Then, we validate a simple theoretical and numerical model by an experiment which consists in measuring over a large dynamic range the transverse profile of a proton beam at the end of a drift space, for various gas pressures. Using this

model, we simulate the transport of the proton beam under our FODO experimental conditions and estimate the magnitude of the scattering-induced halo.

THE SCATTERING PROCESS OF A PROTON BEAM

The Basic Process

We consider, here, the elastic Coulomb scattering of beam particles on the atoms of the residual gas in an accelerator. The probability of collisions is governed by the well known Rutherford differential cross section formula:[6]

$$\frac{d\sigma}{d\theta} = \frac{3.256z^2Z^2}{E^2} \cdot \frac{1}{\sin^3\theta} \cdot \frac{\left(M\cos\theta + \sqrt{M^2 - m^2\sin^2\theta}\right)^2}{M\sqrt{M^2 - m^2\sin^2\theta}} \cdot 10^{-22} \quad (1)$$

where σ is the scattering cross section (in m^2), θ is the scattering angle from the incident direction (in rad), z is the incident particle charge number, Z is the target nucleus charge number, m is the incident particle mass, M is the target nucleus mass, E is the incident particle energy (in MeV).

This formula calls for three comments:

(i) The scattering cross section decreases rapidly with angle (in θ^{-3}), which explains that the scattering process has usually no significant influence on the beam emittance growth.[3] However, the decreasing rate is much smaller than the one of an exponential or a Gaussian shape, which is usually used to describe a beam transverse profile. This implies that, from the halo point of view, a non-negligible number of particles can be scattered at angles greater than the mean divergence of the beam. These particles, under the influence of the beam transport laws, may be rapidly kicked out into the halo region and contribute to beam losses.

(ii) Since the cross section varies as E^{-2}, the scattering process is very important for low-energy particles, which is the case in our experiment (500 keV).

(iii) In most practical applications, the correction term (containing m and M) in formula (1) is considered as constant and equal to 4.

This is justified because, on the one hand, we are dealing with small scattering angles (< 100 mrad), on the other hand, the mass of the incident particle is lower than that of the target nucleus. For example, with $m = 1$, $M = 16$ (proton scattering on an oxygen atom), and for a scattering angle of 100 mrad, the correction term is equal to 3.98 (compared to 4 when $\theta \to 0$ and $M/m \to \infty$). So, for small angle scattering, we can use the simplified differential cross section formula:

$$\frac{d\sigma}{d\theta} = \frac{13z^2 Z^2}{E^2} \cdot \frac{1}{\theta^3} \cdot 10^{-26}. \tag{2}$$

Application to a Proton Beam

Scattering Angle

Let P be the residual gas pressure (in Pascal) in the accelerator vacuum system. Using the perfect gas formula, the number of particles n (m^{-3}) per unit volume is: $n = (N_A P)/(RT)$ where $N_A = 6.02 \cdot 10^{23}$ mol^{-1}, is Avogadro's number, $R = 8.315$ J/mol/K is the perfect gas constant and T is the gas absolute temperature in Kelvin.

The probability per meter (m^{-1}) for a particle to scatter in one collision at an angle between θ and $\theta + d\theta$ is

$$d\text{Prob}(\theta) = d\sigma(\theta) \cdot n. \tag{3}$$

This gives for protons ($z = 1$) in a gas at temperature $T = 300$ K:

$$d\text{Prob}(\theta) = \frac{0.31 Z^2 P}{E^2} \cdot \frac{d\theta}{\theta^3} \tag{4}$$

with P in hPa, E in MeV, θ and $d\theta$ in mrad.

One can notice that, according to Eq. (4), the probability to scatter at an infinitely small angle is infinitely large, which is not physically realistic. In fact, this formula applies only for angles between a minimum angle $\theta_{\min}$ corresponding to a large impact parameter of the order of the atom radius (field screening of nucleus by electrons), and a maximum angle $\theta_{\max}$ corresponding to a small impact parameter of the order of the nucleus radius (charge distribution in the nucleus).

TABLE I   Scattering limit angles for protons on nitrogen

Energy (keV)	p (MeV/c)	θ_{min} (μrad)	θ_{max} (rad)
10^1	4.33	1180	π
10^2	13.7	372	π
10^3	43.3	118	1.35
10^4	137	37	0.43
10^5	445	11.5	0.13
10^6	1670	3.0	0.034

We have[7]: $\theta_{min} = \hbar/(p \cdot a)$ and $\theta_{max} = \hbar/(p \cdot b)$, where $\hbar$ is Planck's constant divided by 2π, p is the incident particle momentum, $a = 1.4a_0 Z^{-1/3}$ is the atom radius, with $a_0 = 0.529 \cdot 10^{-10}$ m the Bohr radius and $b = 1.4A^{1/3} \cdot 10^{-15}$ m is the nucleus radius. Table I gives the values of these extreme angles for protons of different energies, incident on nitrogen nuclei ($Z = 7$, $A = 14$).

From Eq. (4), we calculate the probability, per meter, for a particle to be scattered in one collision at an angle larger than θ_0 ($\theta_{min} < \theta_0 < \theta_{max}$):

$$\text{Prob}(\theta \geq \theta_0) = \int_{\theta_0}^{\theta_{max}} d\text{Prob}(\theta) = \frac{0.155 Z^2 P}{E^2} \cdot \left[\frac{1}{\theta_0^2} - \frac{1}{\theta_{max}^2} \right]. \quad (5)$$

In the case where $\theta_{max}^2 \gg \theta_0^2$, we have

$$\text{Prob}(\theta \geq \theta_0) = \frac{0.155 Z^2 P}{E^2} \cdot \frac{1}{\theta_0^2}. \quad (6)$$

The Transverse Phase-space

We examine now the effect of collisions with the residual gas on the transverse profile of a proton beam. In this section, the beam is assumed to have *zero emittance*, i.e. all proton trajectories are parallel to the propagation axis Oz, as shown in Figure 1(a). The beam transverse profile is further observed through its projection on a given axis, say the horizontal axis Ox (see Figure 1(b)).

We consider a particular proton which is scattered in direction θ, the azimuthal angle ($\theta \in [0, \pi]$), and ϕ, the radial angle ($\phi \in [-\pi, \pi]$), with a probability $\text{Prob}(\theta, \phi) = P1(\theta) \cdot P2(\phi)$, since θ and ϕ are independent variables. $P1(\theta)$ is given by expression (4), $P2(\phi)$ is constant within $[-\pi, \pi]$.
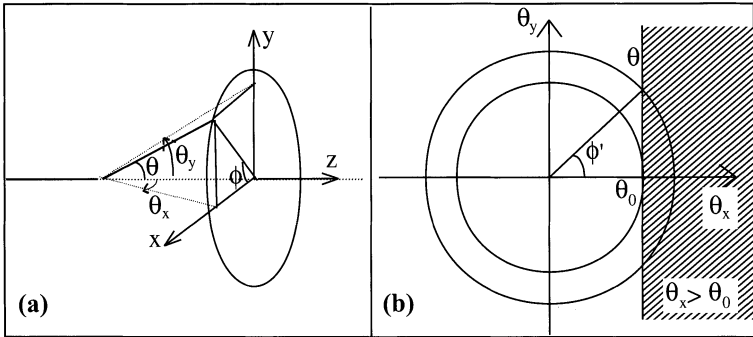
FIGURE 1   Projection of the scattered particle trajectory on the horizontal plane. (a) Spatial view: the particle scatters at an azimuthal angle θ and a radial angle ϕ, which gives an angle θ_x in the horizontal plane and an angle θ_y in the vertical plane. (b) Projection in the transverse space: the probability for θ_x to be greater than θ_0 is represented by the hatched part of the figure.

The angle of the proton trajectory projected onto the horizontal plane xOz is θ_x. We can easily see from Figure 1(b), that $\theta_x = \theta \cdot \cos(\phi)$. The particles scattered at an angle $\theta_x \geq \theta_0$ (hatched part of Figure 1(b)) are those scattered at an azimuthal angle $\theta \geq \theta_0$ with a radial angle ϕ such that $\cos(\phi) \leq \theta_0/\theta$, which means that $-\phi' \leq \phi \leq \phi'$ with $\cos(\phi') = \theta_0/\theta$. We obtain

$$\mathrm{Prob}(\theta_x > \theta_0) = \int_{\max(\theta_0, \theta_{\min})}^{\theta_{\max}} \frac{\phi'}{\pi} \cdot \frac{\mathrm{dProb}(\theta)}{\mathrm{d}\theta} \, \mathrm{d}\theta \qquad (7)$$

where $\phi'/\pi = (1/\pi)\arccos(\theta_0/\theta)$ is the normalised probability for having $\theta_x \geq \theta_0$ for a given θ. Putting $a = \theta_0/\theta$, we have

$$\mathrm{Prob}(\theta_x > \theta_0) = \frac{0.31 Z^2 P}{E^2 \theta_0^2} \int_{\theta_0/\theta_{\max}}^{\min(1, \theta_0/\theta_{\min})} \frac{a}{\pi} \cdot \arccos(a) \, \mathrm{d}a. \qquad (8)$$

We define $G(u)$ as

$$G(u) = 8 \int_0^u \frac{x}{\pi} \cdot \arccos(x) \, \mathrm{d}x$$
$$= \frac{2}{\pi} \left[-u\sqrt{1 - u^2} + 2u^2 \arccos(u) + \arcsin(u) \right], \qquad (9)$$

we have

$$G(1) = 1 \text{ and } G(0) = 0.$$

We finally obtain for the probability relation:

$$\text{Prob}(\theta_x > \theta_0) = \frac{3.9 \cdot 10^{-2} Z^2 P}{E^2 \theta_0^2} \cdot k(\theta_0) \tag{10}$$

with

$$k(\theta_0) = \begin{cases} G(\theta_0/\theta_{\min}) - G(\theta_0/\theta_{\max}) & \text{if } \theta_0 < \theta_{\min}, \\ 1 - G(\theta_0/\theta_{\max}) & \text{if } \theta_{\min} \leq \theta_0 \leq \theta_{\max}, \\ 0 & \text{if } \theta_{\max} < \theta_0. \end{cases} \tag{11}$$

In the case often encountered where $\theta_{\min} \ll \theta_0 \ll \theta_{\max}$, we can use the formula

$$\text{Prob}(\theta_x > \theta_0) = \frac{3.9 \cdot 10^{-2} Z^2 P}{E^2 \theta_0^2}. \tag{12}$$

We have represented, in Figure 2, the variation of $\text{Prob}(\theta_x > \theta_0)$ with θ_0 for different proton energy values, in a monoatomic nitrogen gas $(Z = 7)$ at a pressure of 10^{-6} hPa (this is the same probability as in a molecular nitrogen at a pressure of $5 \cdot 10^{-7}$ hPa). The curves allow one to calculate the scattering-halo development in an accelerator by knowing the beam energy and the gas composition and pressure along the transport line.

The multiple scattering and the plural scattering effects apply only for probabilities greater than 1–10%. In most cases considered here, they do not apply, and the model taking into account single scattering is sufficient.[7] But sometimes, especially for low-energy protons scattered at small angles, in a high-pressure gas over a long distance, we could be obliged to use the statistic-scattering models.

Beam with Small Angular Spread

In the preceding calculation, we have assumed a beam without angular spread. Nevertheless, a real beam has an angular spread (even though,
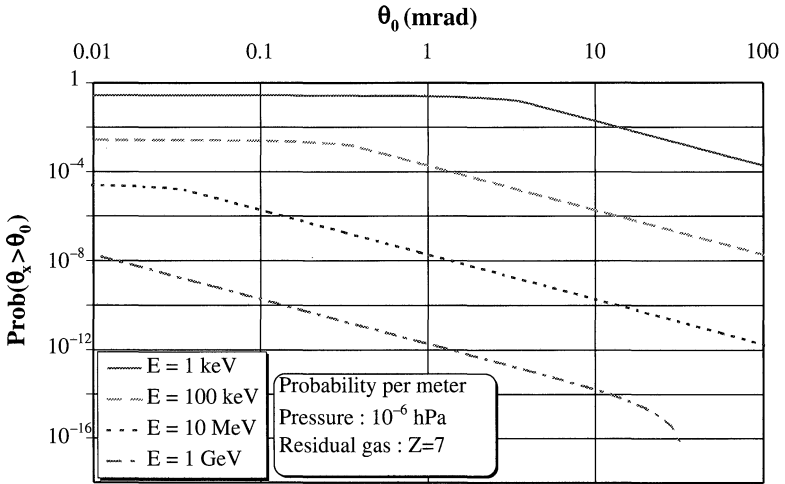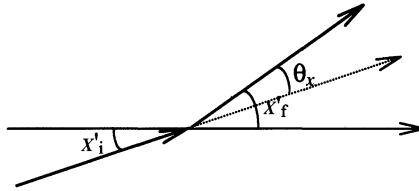
FIGURE 2   Probabilities, per meter, for protons of different energies to scatter at an angle θ_x greater than θ_0 in a monoatomic nitrogen gas at the pressure of 10^{-6} hPa. (See color plate I).

it may be small). A particle trajectory makes an initial non-zero slope x_i' with the beam propagation axis

Assuming $x_i' \ll 1$, and scattering x-projected angle $\theta_x \ll 1$, the final particle slope x_f can be written as

$$x_f' = x_i' + \theta_x. \tag{13}$$

EXPERIMENTAL OBSERVATION

Experimental Results

The experimental set-up is schematically presented in Figure 3. A 500 keV pulsed proton beam, with 500 μs pulse duration, 50 mA peak current, and 1 Hz repetition rate, is delivered by a duoplasmatron
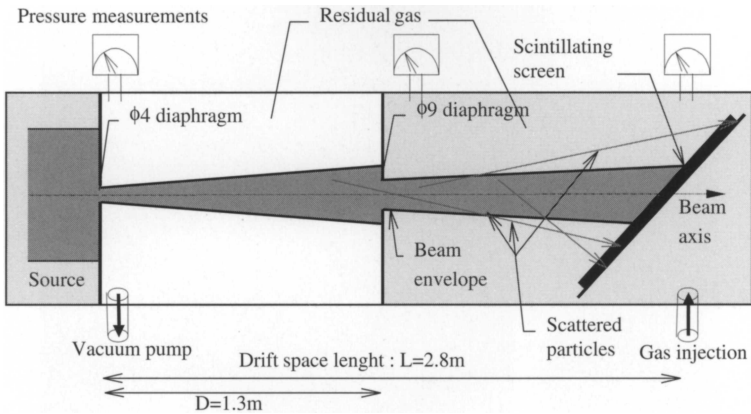
FIGURE 3   Schematic drawing of the experimental set-up.

source. The beam transverse profile is limited by a first diaphragm (ϕ4), with 4 mm diameter, located at the exit of the source, and a second one (ϕ9), with 9 mm diameter, placed downstream 1.3 m from the first one. This diaphragm combination has been adopted to obtain a beam core with homogeneous transverse profile and sharp edges, which ensures accurate observation of the collisional halo. The collimated beam propagates through a drift space towards a scintillating screen located downstream 2.8 m from the first diaphragm (ϕ4) and observed with an intensified CCD camera. This imaging technique is very powerful since it allows density distribution measurements over a very large dynamic range.[8] This scintillating screen is home made. It consists of P47 phosphor crystal powder deposited on a rectangular stainless steel plate. The gas pressure in the evacuated transport line can be changed by injecting nitrogen gas at the level of the scintillating screen. The gas pressure is measured at three locations in the transport line: at the beginning close to the source, in the middle near diaphragm ϕ9, and at the end in the vicinity of the phosphor screen.

The beam profile is observed on a wide dynamic range by progressively moving the phosphor screen towards the beam centre. For each screen position, the light intensification is adjusted to get an analysable image of the halo, as shown on Figure 4.

The total beam profile is, further, restored using the light intensifier calibration curve. Beam profiles are presented in Figure 5 for two different nitrogen gas pressure sets given in Table II.
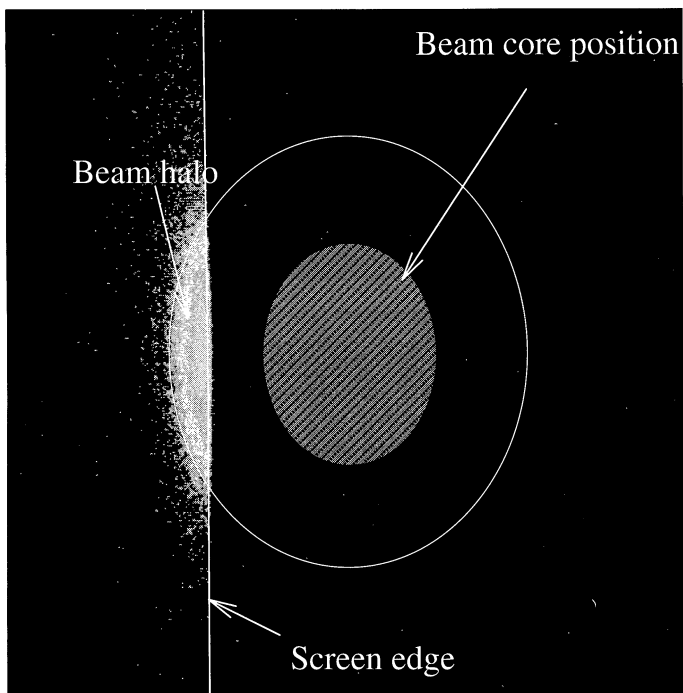
FIGURE 4   Image of the scattering halo with a scintillating screen partly on the path of the beam. (See color plate II).
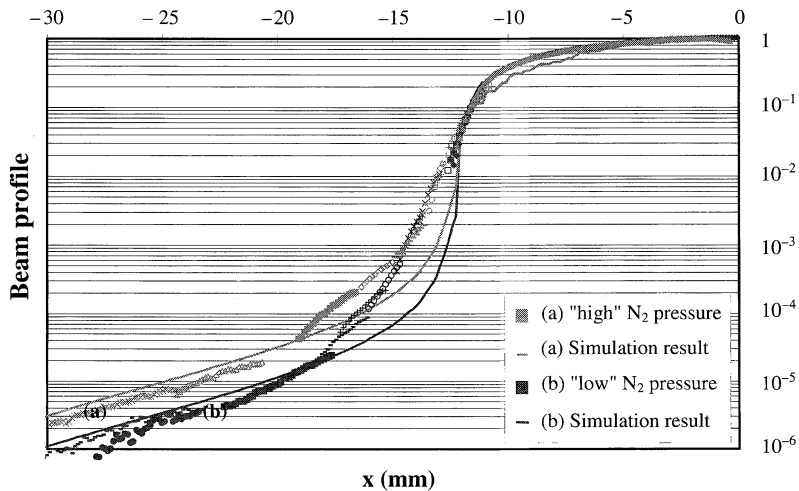

FIGURE 5   Experimental and simulated beam profiles for two different nitrogen gas pressures. (See color plate III).

TABLE II   The two pressure sets in the experiment measured at the beginning, the middle and the end of the drift space

	Beginning	Middle	End
"Low" N_2 pressure (hPa)	$6.4 \cdot 10^{-6}$	$2.0 \cdot 10^{-5}$	$3.2 \cdot 10^{-5}$
"High" N_2 pressure (hPa)	$8.5 \cdot 10^{-6}$	$6.0 \cdot 10^{-5}$	$1.1 \cdot 10^{-4}$

We observe that an increase of the residual gas pressure, by approximately a factor 3 in the second part of the drift space, induces an increase of the beam halo intensity by the same factor. Other measurements, not presented here, obtained for 8 different gas pressures exhibit the same behaviour but more precisely.

Simulation of the Experiment

We have simulated the experiment using the analytical results presented in first section. The simulation method is schematically presented in Figure 6 and described below.

A 2D array (called T, with a size of $N \times M$) contains the beam density distribution digitised in the (x, x') phase space. It is sampled with a step dx in the x direction and a step dx' in the x' direction. $T_{i,j}$ then represents the beam density for x between $((i + 1) - N/2) \, dx$ and $(i - N/2) \, dx$ and for x' between $((j + 1) - M/2) \, dx'$ and $(j - M/2) \, dx'$. This array is initially filled with a homogeneous parallelepiped, corresponding approximately to the measurement of the beam distribution in this (x, x') phase-space presented in Ref. [4] (see Figure 6(1)).

A 1D array (called PP, with a $2M$ size) contains the probability for a particle to scatter at an angle θ_x between $i \cdot dx'$ and $(i + 1) \cdot dx'$, i being the index in the 1D array. We have $PP_i = \{\mathrm{Prob}(\theta_x > [(i + 1) - M] \cdot dx') - \mathrm{Prob}(\theta_x > [i - M] \cdot dx')\} \, dz$. The term $\mathrm{Prob}()$ is calculated using formula (10), dz is the longitudinal processing step length. We note that dx' is the numerical sampling step in both arrays T and PP.

We then simulate the evolution of the beam distribution function. We choose, for that, a processing step length dz and for each step, we determine

– *The beam scattering*, by folding each column of array T (at $x = C^{\mathrm{ste}}$) with the array PP (see Figure 6(2)),
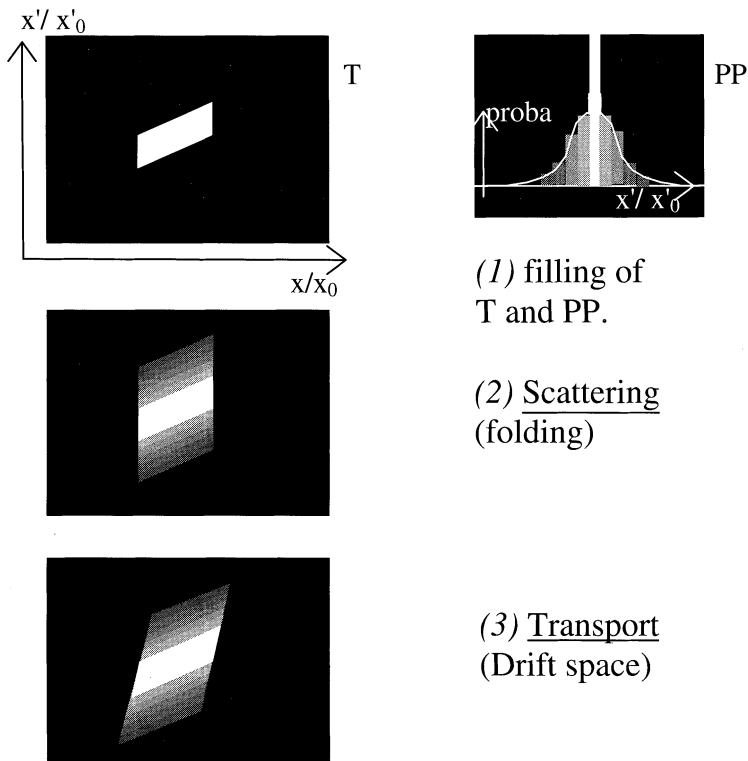
FIGURE 6   Schematics relevant to the simulations. See text for explanations.

— *The beam transport*, by translating each point of the phase-space pattern T along the x axis of a quantity proportional to the co-ordinate x' (that is $x_f = x_i + x' \cdot dz$, $x_f' = x_i'$). This corresponds to the beam transport in a drift space without space-charge effect (see Figure 6(3)).

The difficulty of this study arises from the fact that the particles are scattered in the x' direction of the phase-space, and that we want to observe the scattering effect in the x direction. The coupling between directions x and x' is obtained from the beam transport parameters.

We have assumed here that the scattering probability in the x' direction is independent of the initial slope x_i' of the particle trajectory. In fact, this is not really true, but in the case of small x_i' and small

scattering angles, it is a good assumption to consider the scatter-
ing distribution as being the same as that of a zero divergence particle
beam.

The space-charge effect on the beam-size growth is not taken into
account in our simulation code. Thus, in order to compare precisely the
experimental and simulation results, we have multiplied the x axis of the
profile obtained from the simulation by a factor 1.7 to obtain the same
beam-core diameter for experiment and simulation. The simulation
results are also shown in Figure 5, they have been established for the
pressure conditions of the experiment. However, pressure values at
intermediate positions along the transport line have been determined
by linear interpolation between the three measurements.

Although the space-charge effect is roughly considered, the particle
motions in the x and y directions are assumed to be independent, the
detailed initial beam emittance and the exact gas pressure distribution
are not taken into account in our simulation code, the calculated results
are in quite good agreement with the experimental data, especially
far from the beam centre, beyond 1.5 times the beam-core radius. We
observe, however, a discrepancy between the measured and simulated
transverse distributions in the halo region close to the beam-core
(between 1 and 1.5 times the beam-core radius). This can be explained
by the crude description of the initial beam emittance in the simulation,
which leads to sharper beam edges than for the experiment. This experi-
mental "nearby" halo, whose shape seems to be independent of the gas
pressure, may also be created by space charge effect within the beam.
Nevertheless, we can conclude that our simple model of beam scattering
on the residual gas is good enough to allow predictions on the scattering
halo formation in the FODO experiment, or in a high intensity linear
accelerator.

SIMULATION OF THE FODO EXPERIMENT

We now consider the simulation of a proton beam transport in our
FODO experiment.[4] To simplify the simulation, the beam is assumed to
be transported in a uniform focusing channel of 10 m in length. From
the scattering point of view, it is nearly equivalent to the transport in a
periodic focusing channel. Moreover, we assume that the proton beam

has a Kapchinsky–Vladimirsky (K–V) distribution[9] in the transverse phase-space, which means that the emittance ellipse in the (x, x') phase-space is homogeneous. In addition, we consider that the beam is matched in the channel. This means that, in the K–V conditions, each beam particle moves in a harmonic-oscillator potential well. The other beam properties are: a proton beam energy of 500 keV, a maximum angular spread $x_0' = \pm 4$ mrad, a residual gas of monoatomic nitrogen ($Z = 7$) and a betatron wavelength of 2 m. The transverse beam size is a parameter which does not influence the simulation results.

The simulation method is nearly the same as that used for the drift space and described above. The only differences are the following:

– The array T is initially filled with a homogeneous disc, corresponding to the projection of the beam K–V distribution in the transverse phase space.
– We choose a processing step length, dz, much smaller than the betatron oscillation wavelength L. During one step, we can verify that the probability for a particle to scatter to an angle greater than dx' is much smaller than unit ($= 3 \cdot 10^{-4}$ for a 10^{-5} gas pressure), justifying the use of single scattering probabilities rather than multiple scattering one.
– The beam transport, for each step dz, consists in rotating the phase-space pattern T an angle $\theta = 2\pi(\mathrm{d}z)/L$. This corresponds to beam transport in a harmonic-oscillator potential well.

The beam profile obtained at the exit of the channel is represented in Figure 7, for different pressure values. We can notice that the collisional halo develops very far away from the core.

DISCUSSION ABOUT INFLUENCE OF SPACE-CHARGE

When the beam is space-charge driven, 2D phase-space beam distributions are no longer ellipses, but tend to become rectangles. In that case, particle trajectories (iso-hamiltonian curves) are not ellipses in phase-space, but are curves whose shape depends on the beam distribution through the space-charge potential.

When the beam is space-charge dominated, it can be assumed that iso-hamiltonian curves in $(x/x_0, x'/x_0')$ are nearly rectangles[10]
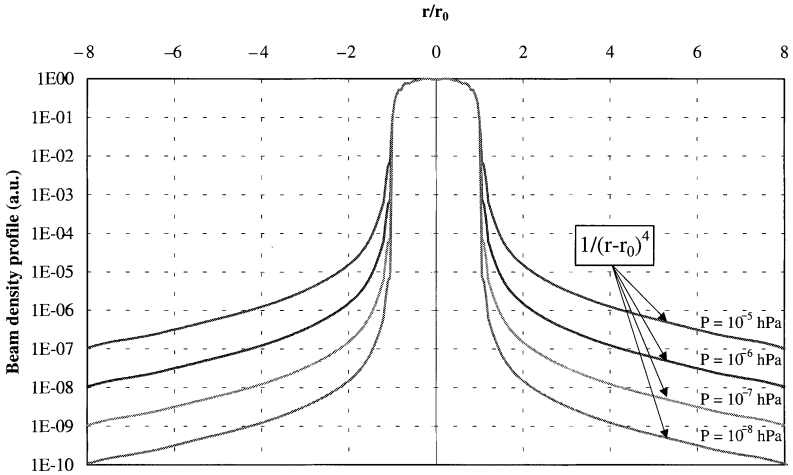
r/r$_0$

FIGURE 7   Influence of the scattering process on the beam profile. The different curves correspond to different gas pressures. The tails, induced by the scattering, decrease in $1/(r - r_0)^4$. (See color plate IV).

(as represented in Figure 8). In that case, in order to get the same amplitude, a particle needs to be scattered to an angle larger than the one that would have been necessary with no space-charge force (where ellipses are the iso-hamiltonian curves).

This situation can be seen in another way: When there are space-charge forces, more external focusing forces are needed to transport the beam with the same size. In that case, the confinement potential well is deeper, and the kinetic energy (gained in a collision) needed to reach the same amplitude is higher. This will decrease the residual gas scattering halo.

If k_0 is the external focusing phase advance per meter, and η is the tune depression factor of the beam, then

$$x_0' = \eta k_0 \cdot x_0.$$

Rd is the homogenous-part beam size, and ΔR is its border size, then
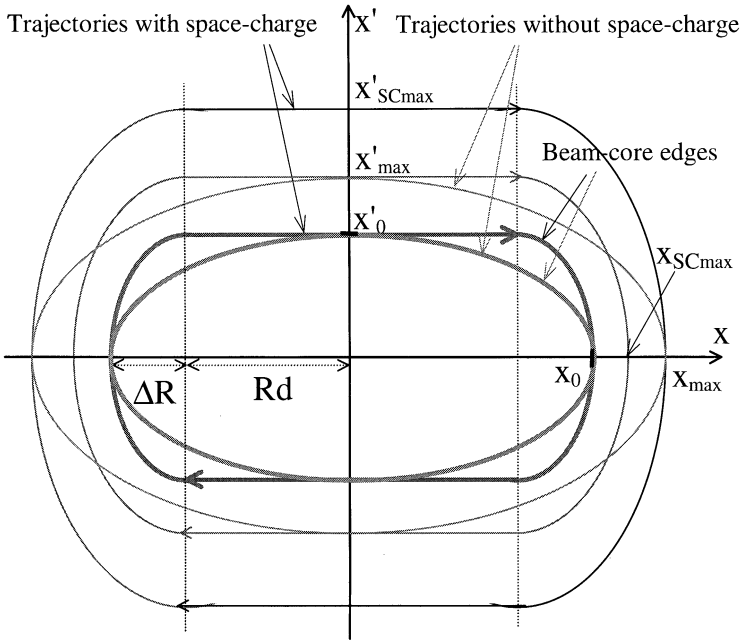
$$x_0 = Rd + \Delta R.$$

FIGURE 8   Beam shape and particle trajectories around a beam with: ■ no space-charge forces (ellipses, in red), ■ space charge forces (quasi-rectangles, in green). The scattering angle necessary to get an amplitude x_{max} is larger with space-charge than without space-charge. (See color plate V).

If we assume* that particles outside the beam are only subject to external forces, we can write

$$\Delta R = \frac{x_0'}{k_0},$$

which gives $Rd = x_0 - (x_0'/k_0) = x_0(1 - \eta)$.

Two particles scattering to the same angle x_{max}' will not reach the same amplitude depending on whether we take into account space-charge (x_{SCmax}) or not (x_{max}). We have

$$\frac{x_{SCmax}}{x_{max}} = \frac{Rd + x_{max}'/k_0}{x_{max}'/k_0} = \frac{Rd + \eta x_{max}}{x_{max}} = \eta + (1 - \eta) \cdot \frac{x_0}{x_{max}}.$$

---

* The logarithm contribution of the space-charge potential can be neglected.

The space-charge decreases the particle amplitude by a factor between 1 (close to the core when $x_{max} = x_0$) to η (far from the core when $x_{max}/x_0 \to \infty$).

The amplitude density is increased because the scattering x-slope range for which particles have amplitudes between x and $x + dx$ is larger with space-charge than without space-charge. This amplification factor is

$$\frac{dx_{SCmax}}{dx_{max}} = \eta + (1 - \eta) \cdot \frac{x_0}{x_{max}}.$$

Ignoring space-charge when calculating the density leads to a too high value. The calculations presented in Figure 7 must therefore be corrected (see Figure 9) to take space-charge into account. This can be done by the following transformations:

$$n(x) = \frac{n(x)}{(\eta + (1 - \eta) \cdot (x_0/x))},$$
$$x = x \cdot (\eta + (1 - \eta) \cdot (x_0/x)).$$

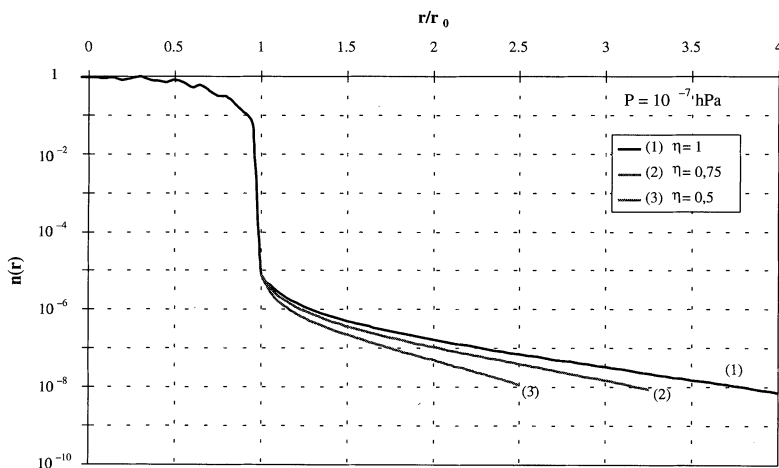Due to the profile variation in $1/r^4$ far from the core, the beam far-halo density will be decreased by a factor η^3.

FIGURE 9   Space-charge influence on the particle amplitude distribution. (See color plate VI).

BEAM LOSSES IN A HIGH INTENSITY TRISPAL LINAC

TRISPAL Linac

The proton TRISPAL linac[11] is composed of 4 different parts (Figure 10):

(1) ECR source (SILHI, 100 keV, 40 mA (up to 100 mA) protons),
(2) RFQ (from 100 keV to 5 MeV),
(3) DTL-CCDTL (from 5 MeV to 100 MeV),
(4) CCL (from 100 MeV to 700 MeV).

The residual gas in the linac will be responsible of halo formation.

Residual gas scattering is more important at low energy than at high energy, firstly because of the scattering cross section varying in (kinetic energy)$^{-2}$ and secondly because of the higher gas pressure close to the source.

Nevertheless, because the beam size and normalised emittance are kept constant along the acceleration, the beam angular spread decreases as $1/p$ (p being the particle momentum). In consequence, the scattering angle allowing to reach the halo decreases as $1/p$.

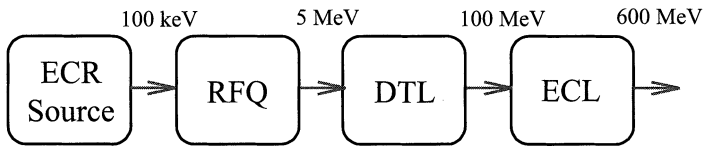In addition, as shown in Table III, the acceptable loss rate decreases with energy.

FIGURE 10   TRISPAL linac.

TABLE III   Proton losses inducing a 2.8 mrem/h gamma dose at 1 m from the linac after 1 h decay

Energy (MeV)	10	20	50	100	200	500	1000
Acceptable losses (nA/m)	200	15	2.5	1	0.2	0.05	0.03

Basic Model

Let us modelize the TRISPAL linac with a continuous focusing channel, increasing smoothly the matched beam energy from 10 MeV to 1 GeV. The beam RMS normalised emittance is constant along the transport: $\varepsilon_{nRMS} = 2.4 \cdot 10^{-7}\,\pi \cdot m \cdot rad$. The RMS-beam size is kept constant too: $\sigma_x = 3$ mm. Linac pipe has a $\phi = 28$ mm diameter. Space-charge tune depression factor used in this model is $\eta = 1$ (no space-charge forces).

Particle trajectories in $(x/\sigma_x, x'/\sigma_{x'})$ phase-space are circles. σ_x is the RMS-beam size in x direction and $\sigma_{x'}$ is the beam RMS-divergence in the same direction. A particle scattering to an angle $x' > x'_{max}$ will be directly lost (Figure 11) (after $1/4$ of betatron period) where

$$x'_{max} = \frac{\phi \sigma_{x'}}{2\sigma_x}.$$

A particle which scatters to an angle $x' >$ some $\sigma_{x'}$, will enter the halo.
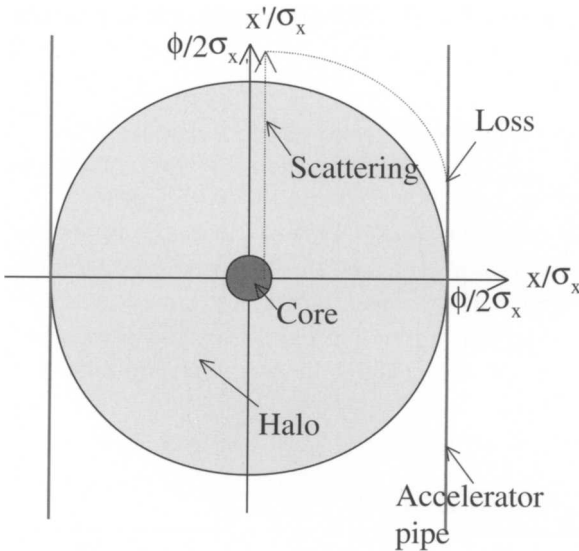

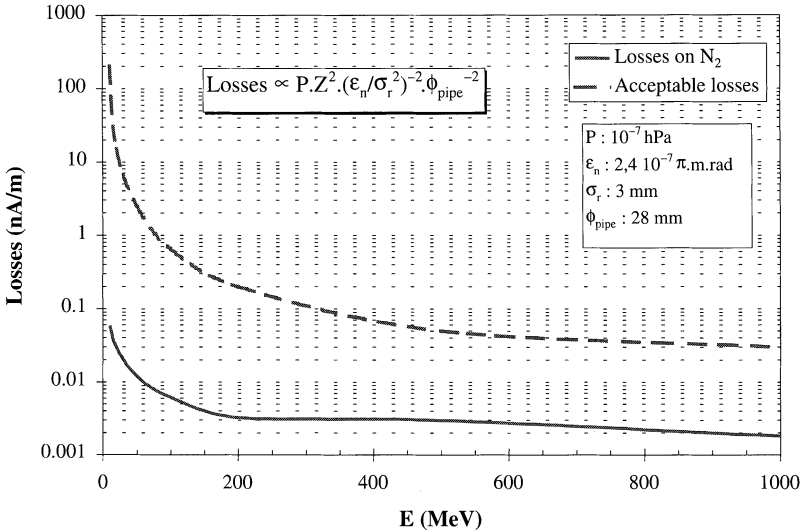FIGURE 11   Particle scattering inducing loss.

FIGURE 12   Direct losses in residual gas for TRISPAL linac.

On Figure 12 direct losses of a 100 mA beam have been represented. They are compared with acceptable losses given by Table III. The molecular nitrogen $(Z = 7)$ residual gas pressure is 10^{-7} hPa.

Remarks

- As shown on Figure 12, losses are proportional to the gas pressure, the square of charge number, and inversely proportional to the square of the angular spread and the pipe diameter.
- Losses in hydrogen gas $(Z = 1)$ are 49 times lower than in nitrogen. In fact, the partial pressures of all gases, and especially of heavy rare gases or hydrocarbon, have to be taken into account.
- The gas pressure is not constant over the accelerator. Between vacuum pumps, the gas pressure can be several times the one at the pump position.
- All "with gas" elements will induce localised losses.

Extension of the Basic Model

In the basic model, some assumptions have been made. Let us have a look on their influence.

Space-charge influence   With space-charge ($\eta < 1$), as seen previously, scattered particles do not have the same phase advance per meter than those of the core. This increases the maximum angle beyond which the particle is lost. Direct losses are then reduced by a factor $1/\eta^2$.

Periodic transport   In a real linac, the transport channel is not continuous but periodic. The beam size is then oscillating around a mean value, and has a higher value in the focusing quadrupoles. In the basic model, continuous losses have been considered while they are actually localised in quadrupoles.

Non-direct Losses

Results of calculations shown in Figure 13 take the direct losses into account. But many scattered particles are not lost but enter into the beam halo, and are potential losses which are dangerous in case of mismatch and misalignment.

For example, in TRISPAL linac, assuming a mean energy gain of 1 MeV/m, the beam fraction stored from an energy of 10 MeV to the final energy of 600 MeV, in a 10^{-7} hPa nitrogen gas pressure, having an amplitude between 25 and 28 mm (very close to the pipe) is 1.4 nA, which is 30 times the acceptable losses per meter at that energy!!

In case of misalignment and mismatch, or a change of accelerator acceptance (for example in matching sections), the beam will undergo localised losses.
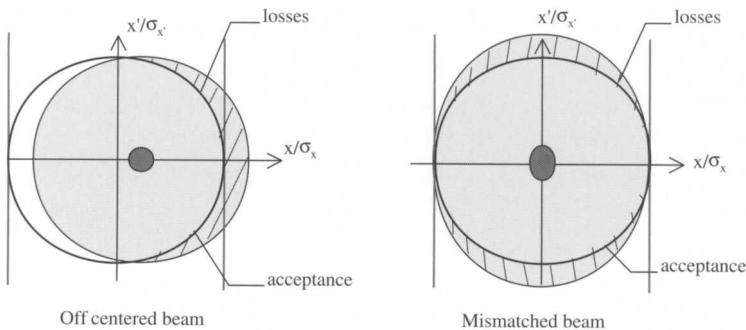

FIGURE 13   Basic representation of the effect of some transport errors on beam losses.

CONCLUSIONS

In a linear accelerator, the scattering process can be very significant, particularly in the low-energy part and near the source, where the vacuum pressure is generally high. The transport of this "collisional halo" through the high-energy sections, where its effects may be serious, has to be studied. A means of eliminating the halo before it reaches these sections has to be found.

We notice that the larger the angular spread of the beam is, the less important the scattering effects are. This means that, for a given emittance, it is better to transport a small-size beam, with large angular spread. It also leads to an increased tune depression factor η.

Losses can be reduced:

– By decreasing the residual gas pressure and particularly of heavy gas molecules (losses $\propto P \cdot Z^2$),
– by using strong focusing forces (losses $\propto \sigma_x^4 \cdot \eta^4$),
– by increasing the pipe diameter (losses $\propto \phi^{-2}$), even if this is not very efficient for this kind of losses.
– by controlling carefully the beam matching and alignment. The acceptance should not decrease in order to avoid localised losses.

As a consequence of the huge diffusion at low energy, it seems interesting to clean the beam at low and medium energies.

References

[1] J.M. Lagniel, Chaotic behaviour induced by space-charge, EPAC 94, London, Great Britain, 27 June–1 July, 1994, Conf. Proc. Vol. 2, p. 1177.
[2] C. Chen and R.A. Jameson, Self-consistent simulation studies of periodically focused intense charged-particle beams, *Phys. Rev.* **E52** (1995) 3074.
[3] M. Reiser, *Theory and Design of Charged Particle Beams*, J. Wiley & Sons, p. 539.
[4] P.-Y. Beauvais *et al.*, Studies on halo formation in a long magnetic quadrupole FODO channel – First experimental results, PAC 95, Dallas, Texas, USA, 1–5 May, 1995.
[5] J.M. Lagniel, Chaotic behavior and halo formation from 2D space-charge dominated beams, *Nucl. Instr. Meth.* **A345** (1994) 405.
[6] H. Straub, H. Bethe, J. Ashkin, N.F. Ramsey and K.T. Bainbridge, *Experimental Nuclear Physics*, Vol. 1, E. Segre, Editor, p. 251.
[7] J.D. Jackson, *Classical Electrodynamics*, second edition, J. Wiley & Sons, p. 650.
[8] N. Pichoff, G. Haouat *et al.*, Experimental study of the ELSA electron-beam halo, *2nd European Workshop on Beam Diagnostics and Instrumentation for Particle Accelerators*, Travemünde, Germany, 28–31 May, 1995, Conf. Proc. p. 63.

[9] I.M. Kapchinsky and V.V. Vladimirsky, *Proc. International Conf. on High Energy Accelerators*, CERN, Geneva, 1959, p. 274 ff.

[10] N. Pichoff *et al.*, Stationary distribution of space-charge driven continuous beam, Note DAPNIA/SEA 98/43.

[11] J.M. Lagniel, High Intensity Linac Study in France, LINAC 98, Chicago, August 23–28, 1998.